Journal of Drug Delivery Science and Technology 95 (2024) 105540

Contents lists available at ScienceDirect

Journal of Drug Delivery Science and Technology

journal homepage: www.elsevier.com/locate/jddst

S-protected thiolated surfactants enhancing surface properties of lipid-based nanocarriers

Gennaro Balenzano [a], Giuseppe Francesco Racaniello [a], Miriam Domenica Panzarino [a], Patrick Knoll [b], Martyna Truszkowska [b], Valentino Laquintana [a], Andreas Bernkop-Schnürch [b], Nunzio Denora [a,*]

[a] Department of Pharmacy – Pharmaceutical Sciences, University of Bari Aldo Moro, Orabona St. 4, Bari, 70125, Italy
[b] Department of Pharmaceutical Technology, Institute of Pharmacy, University of Innsbruck, Innrain 80/82, 6020, Innsbruck, Austria

ARTICLE INFO

Keywords:
Thiolated surfactant
Lipid-based nanoparticle
Surface decoration
Mucoadhesion
Mucodiffusion
Cellular uptake

ABSTRACT

This work aimed to investigate the influence of surface decoration of orally administered lipid-based nanocarriers (LNCs) through S-protected thiolated surfactant on key properties such as mucodiffusion, adhesion and cellular uptake. This comparative study with simple thiolation was performed on chemically modified polyoxyethylene stearyl ether (PSE) surfactant with different PEG chains exhibiting free thiol groups, which were subsequently protected by mercaptonicotinic acid or cysteine. Successively, nanostructured lipid carriers (NLCs) and solid lipid nanoparticles (SLNs) were decorated with thiolated PSE surfactants and their impact on the formulations was evaluated through in-vitro studies on intestinal mucosa. Characterization studies on mucus diffusion and adhesion were first performed to assess the ability of LNCs to reach the adsorption epithelia. Then, cellular uptake and endosomal escape analysis showed the successful performance of the cysteine-protected thiolate surfactant-based samples in being the more taken up among the investigated decoration and to evade from the adopted endosome model. Furthermore, the results confirmed that the PEG chain length determines the efficacy of the produced systems, showing that shorter polymer chain length corresponds to better cellular uptake. Hence, considering the obtained results, the samples resulting from the adoption of PSE_{10}-Cys could represent interesting nanosized vehicles for drug delivery in mucosal tissues.

1. Introduction

In recent years, pharmaceutical research has focused on the development of increasingly efficient drug delivery systems (DDSs), with lipid-based nanocarriers (LNCs) emerging as an attractive alternative for the improvement of therapeutic outcomes. LNPs offer a versatile platform for encapsulating and delivering a wide range of pharmaceutical agents, from small-molecule drugs to nucleic acids and proteins [1,2]. Nevertheless, the effectiveness of these formulations lies in their surface properties, which have a significant impact on overcoming physiological barriers and being properly adsorbed, particularly when considering the oral route of administration and the properties of the intestinal epithelium [3,4]. Various approaches have been exploited bioinert surfaces, charge-converting surfaces, and adsorption-enhancing surfaces, to bypass the mucosal barrier and improve cellular uptake [5–7]. Among these, superficial thiolation has already been proven to modify and increase the mucodiffusive, mucoadhesive and cellular uptake properties of LNCs [8]. Indeed, the thiolation of the hydrophilic head group of surfactants such as polyoxyethylene stearyl ether (PSE), with their lipophilic tails firmly anchored in the lipid phase of nanocarriers, guarantees the induction of several active internalization pathways. Nevertheless, the instability of the –SH group under physiological conditions and the easy interaction with the cysteine-rich subdomains of the mucus layer, prevents the thiolated formulation from reaching the epithelial membrane [9].

This work aimed to take advantage of different S-protected moieties for the surface decoration of LNCs and to compare their potential influence on mucoadhesion, mucodiffusion, and cellular uptake. The introduction of disulfide bonds between thiomers and MNA improves stability and increases reactivity for thiol/disulfide exchange reactions, resulting in a preactivated S-protected compound [10,11]. However, high reactivity may hinder penetration into deeper mucus regions,

* Corresponding author.
E-mail address: nunzio.denora@uniba.it (N. Denora).

https://doi.org/10.1016/j.jddst.2024.105540
Received 10 January 2024; Received in revised form 29 February 2024; Accepted 5 March 2024
Available online 6 March 2024

suggesting that less reactive S-protection could potentially exhibit even higher mucodiffusion and adhesion. Hence, a -S-Cys substructure was further investigated for its reduced reactivity and inherent properties, resulting in a safer and more efficient method of delivering drugs through the mucosa and reaching the intestinal epithelium [12].

For this purpose, modified PSE surfactants with either 10- or 100-unit PEG chains ($PSE_{10/100}$) were produced exhibiting free –SH groups or groups S-protected by MNA and Cys. Then, LNCs, namely nanostructured lipid carriers (NLCs) and solid lipid nanoparticles (SLNs), were developed and characterized in terms of size, polydispersity index, and ζ-potential and subsequently examined *in vitro* regarding the cytotoxicity of the systems and their fate in intestinal mucosa and for endosomal escape is considered.

2. Materials and methods

2.1. Materials

Polyoxyethylene (10) stearyl ether (PSE_{10}) and Polyoxyethylene (100) stearyl ether (PSE_{100}), minimum essential medium (MEM), Tris buffer, resazurin sodium salt, sodium chloride (≥99.5%), sodium-borohydride, Triton-X 100, 4-nitrophenyl chloroformate (4-PN), triethylamine (TEA), N,N′-Dimethylformamide (DMF), L-Cysteine (Cys), 6-thionicotinic acid/6-mercaptonicotinic acid (6-MNA), 5,5′-dithiobis(2-nitrobenzoic acid) (DTNB), Pluronic F-127 (Poly(ethylene glycol)-block-poly(propylene glycol)-block-poly(ethylene glycol)), Pluronic F68 (Polyoxyethylene-polyoxypropylene block copolymer) were obtained by Sigma-Aldrich Italy (Milano, Italy). HEPES buffered saline (HBS) and Hoechst 33528 were purchased from ThermoFisher Scientific (Waltham, Massachusetts, USA). Lumogen F Red 300 (LGR) was a kind gift from BASF (Ludwigshafen, Germany). Crodamol GTCC (Caprylic/Capric Triglyceride) was obtained by Croda (Germany). Lipoid S100 (soy lecithin) was a gift from Lipoid GmbH (Ludwigshafen, Germany). Miglyol 840 (propylene glycol dicaprylate/dicaprate) and Witepsol E85 (Glycerolester of C8 to C18 fatty acids) were received by IOI Oleo GmbH (Witten, Germany). Precirol ATO5 (Glyceryl distearate) was a gifted by Gattefossè (St. Priest, France). Capmul GDB (glyceryl dibehenate) was supplied by Abitec (Columbus, USA) as free samples,.TEGO Care CG90 (Cetearyl Glucoside) was a gift from Evonik (Hamburg, Germany). Cetyl Palmitate and Paraffin wax were obtained by Carl Roth (Karlsruhe, Germany).

2.2. Synthesis and purification of thiolated $PSE_{10/100}$

PSE_{10} and PSE_{100} were chemically modified to generate the three generations of thiolated surfactants, namely first-generation PSE_{10}-SH and PSE_{100}-SH, second-generation MNA S-protected surfactants PSE_{10}-MNA and PSE_{100}-MNA and third generation of Cys S-protected PSE_{10}-Cys and PSE_{100}-Cys.

2.2.1. Synthesis of first generation $PSE_{10/100}$: $PSE_{10/100}$-SH

As shown in Fig. 1A, PSE_{10}-SH and PSE_{100}-SH were obtained through a 2-steps process [13]. Briefly, in the first step, hydroxyl groups (-OH) in $PSE_{10/100}$ were substituted with 4-PN to obtain the $PSE_{10/100}$-PN. In detail, 10.4 mmol of 4-PN and 7.5 mmol of $PSE_{10/100}$ were separately dissolved in anhydrous CH_2Cl_2. Subsequently, 1–2% (v/v) TEA and the solution of 4-PN were added in this order to the unmodified $PSE_{10/100}$. The reaction was left to be occurred overnight. Then, the mixture was dried through Rotavapor® R-200 (BUCHI Italia s.r.l, Italy). In the second step, $PSE_{10/100}$-PN was modified by substitution with the desired thiolated moiety. Briefly, Cys and the $PSE_{10/100}$-PN were dissolved in distilled water at pH 5. Cys was added with a molar ratio of 0.023 mmol $PSE_{10/100}$-PN/0.041 mmol Cys and the pH was adjusted to 8 by the addition of 5 M NaOH solution. The reaction was magnetically stirred for 2 h at room temperature, under an N_2 atmosphere, in dark conditions. The reaction was stopped by raising the pH to 5 using a 1 M HCl solution. The final product was dialyzed against demineralized water for three days using different dialysis tubes for PSE_{10} (CE, MWCO 100–500 Da, Spectra/Por®) and PSE_{100} (CE, MWCO 500–1000 Da, Spectra/Por®) (Spectra/por® Dyalisis Membrane, Biotech CE Trial Kit). The dialyzed products were frozen and lyophilized using Christ Alpha 1–4 LSC (Martin Christ Gefriertrocknungsanlagen GmbH, Germany) under reduced pressure (0.018 mbar) at −50 °C for 24 h. The products were stored at room temperature in dark conditions.

2.2.2. Synthesis of second generation $PSE_{10/100}$: $PSE_{10/100}$-MNA

To obtain second-generation products, the reaction was conducted using $PSE_{10/100}$-SH as a reagent. For this reaction step 6,6′-dithionicotinic acid (6,6′-DTNA) was prepared via the oxidative coupling of the monomer with hydrogen peroxide (H_2O_2) as previously reported [14]. Briefly, 2 g of 6-MNA were dispersed in 50 mL of demineralized water by sonication for 1 h. Subsequently, the pH of the reaction mixture was adjusted to 8.0 using 5.0 M NaOH solution. The mixture was stirred continuously for 60 min, resulting in a slightly yellowish-clear solution. To obtain a colorless solution of 6,6′-DTNA, 2.5 mL of H_2O_2 (30%, v/v) was added dropwise while maintaining the pH at 8. The product was then lyophilized and stored under vacuum at room temperature. In the second step, the 6-MNA was coupled to the thiolated polymer through a disulfide exchange reaction. 30 mg of 6,6′-DTNA were dissolved in 5 mL of water and pH was adjusted to 8 by 1 M NaOH solution. Then, 60 mg of solid $PSE_{10/100}$-SH were added and the mixture was stirred overnight at room temperature while maintaining the pH at 8, in dark condition. The

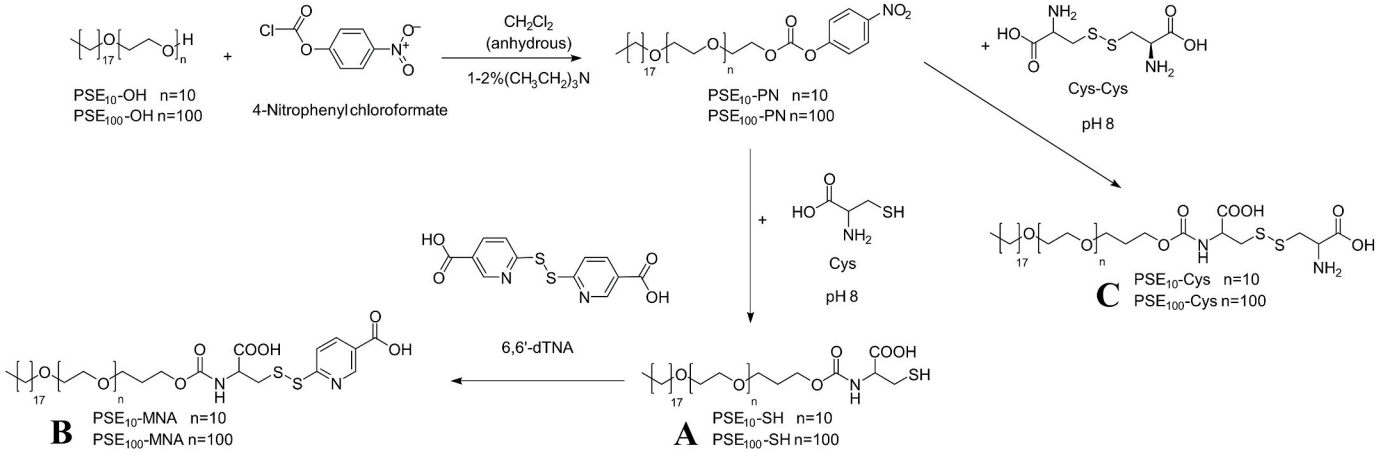

Fig. 1. Reaction scheme for the synthesis of $PSE_{10/100}$-SH (**A**), $PSE_{10/100}$-MNA (**B**), and $PSE_{10/100}$-Cys (**C**).

product was purified via dialysis as described above against demineralized water for 3 days. The final products (PSE_{10}-MNA and PSE_{100}-MNA) (Fig. 1B) were obtained after lyophilization and stored in dark conditions at room temperature.

2.2.3. Synthesis of third generation $PSE_{10/100}$: $PSE_{10/100}$-Cys

The synthesis was conducted similarly as described in section 2.2.1, using L-Cystine as a thiolated moiety to obtain $PSE_{10/100}$-Cys (Fig. 1C). Briefly, in the first step, hydroxyl groups (-OH) in $PSE_{10/100}$ were substituted with 4-PN. In detail, 10.4 mmol of 4-PN and 7.5 mmol of $PSE_{10/100}$ were separately dissolved in anhydrous CH_2Cl_2. Subsequently, 1–2% (v/v) TEA and the solution of 4-PN were added in this order to the unmodified $PSE_{10/100}$. The reaction was left to be occurred overnight. Then, the mixture was dried through Rotavapor® R-200. In the second step, -PN was replaced by the desired thiolated moiety. Briefly, L-Cystine and $PSE_{10/100}$-PN were dissolved in distilled water at pH 5. The Cys was added with a molar ratio of 0.023 mmol $PSE_{10/100}$-PN/0.041 mmol Cys and the pH was adjusted to 8 by the addition of 5 M NaOH solution. The reaction was magnetically stirred for 2 h of stirring at room temperature, under an N_2 atmosphere, in dark conditions. The reaction was stopped by raising the pH to 5 using a 1 M HCl solution. The final product was dialyzed against demineralized water for three days in different dialysis tubes for PSE_{10}-Cys (CE, MWCO 100–500 Da, Spectra/Por®) and PSE_{100}-Cys (CE, MWCO 500–1000 Da, Spectra/Por®). The dialyzed product was frozen and lyophilized as described above.

2.3. Characterization of compounds

^{1}H NMR spectra were used to confirm the molecular structure of $PSE_{10/100}$, $PSE_{10/100}$-SH, $PSE_{10/100}$-PN, $PSE_{10/100}$-MNA, $PSE_{10/100}$-Cys. ^{1}H NMR spectra were carried out on an Agilent VNMRS 500 MHz spectrometer, using $CDCl_3$ as solvent. Chemical shifts were referenced by using the residual solvent signal of $CDCl_3$ at 7.29 ppm.

2.4. Quantitative analysis of thiol and disulfide content

Ellman's test was used to determine the degree of thiolation as described by Racaniello et al. [15]. The amount of thiol groups was calculated by using a standard curve of a known amount of Cys prepared in the same way as the samples, whereas the disulfide contents were calculated after reduction with $NaBH_4$ [16]. In detail, 1.0 mg of each sample was dissolved in 500 μL of 0.5 M phosphate buffer (PBS) pH 8.0 and 500 μL of Ellman's reagent, containing 3 mg of DTNB in 10 mL of 0.5 M PBS, pH 8.0, were added. After 90 min of incubation, protected from light and at room temperature, the samples were centrifuged for 5 min at centrifugated in an Eppendorf Minispin (Eppendorf, Germany) at 9000 g for 2 min. Afterward, 100 μL were transferred to the microplate reader Tecan infinite® M200 spectrophotometer (Tecan, Austria) for quantification, and absorbance was measured at 450 nm. In parallel, calibration curves were established using a stock solution of 1 mg/mL of Cys as control. To determine the efficacy of the reaction on the surfactant backbone, the amount of free or oxidized sulfide group was quantified. Thereafter, 1 mg of the sample was dissolved in 500 μL 0.5 M tris-buffer and 1 mL of a fresh sodium-borohydride solution (4% w/v) was added to the resulting solution to reduce the disulfide bonds. The samples were incubated at 37 °C for 1 h and the reaction was stopped by adding 250 μL 5 M HCl drop by drop, thereby neutralizing the excess of the reducing agent. Then, 1 mL of PBS 1 M at pH 8 was added with 250 μL fresh prepared Ellman's reagent. The mixture was incubated at room temperature for 120 min. Subsequently, 100 μL the obtained mixture was transferred in the microplate reader spectrophotometer, and the absorbance of the samples was recorded at 450 nm, in comparison with the control. All the experiments were made in triplicate.

2.5. Preparation of NLCs and SLNs

NLCs and SLNs were prepared by melt emulsification followed by ultrasonication [17]. Combinations of lipids were prepared and characterized and the most promising formulations of NLCs and SLNs were used for further studies. Their composition is shown in Table 1.

To evaluate the most promising formulation, the lipid nanoparticles were firstly prepared using unmodified PSE_{10}. Briefly, the components were melted at 70 °C, and then 5 mL of ultrapure water, warmed up to the same temperature, was added. The particle dispersion was immediately sonicated for 2.5 min by Ultrasonic Processor UP-200 H (Dr. Hielscher Ultrasonics GmbH, Teltow, Germany) at 80% amplitude and 0.75 Hz, then stirred on ice to allow the formation of NLCs and SLNs, respectively. Water that evaporated during ultrasonication was replenished at a final concentration of 3% (w/v) of particles in water. Afterward characterization and identification of the best performing composition, the same procedure was applied with the equal amount of thiolated surfactants, using $PSE_{10/100}$-SH, $PSE_{10/100}$-MNA, and $PSE_{10/100}$-Cys. Further, for quantification purposes in the following studies, SLNs and NLCs were additionally loaded with 0.5% (m/v) of LGR by dissolving the LGR in the lipid phase of SLNs and NLCs. After cooling NLCs and SLNs on ice, the nanocarriers were stored in a fridge until further use.

2.6. Size distribution, polydispersity index, and ζ-potential

Size distribution, polydispersity index, and ζ-potential of the particles were determined via dynamic light scattering technique (Malvern Zetasizer ZSP, UK). The ζ-potential was measured using a palladium electrode-equipped dip cell (Malvern Universal Dip Cell, Worcestershire, UK). All the samples were analyzed after proper dilution in demineralized water and incubation for 5 min at 37 °C in an Eppendorf ThermoMixer® C (Eppendorf, Germany). The experiments were conducted at 37 °C.

2.7. Mucus purification

The mucus was freshly collected from pig intestines obtained from a local slaughterhouse. The mucus thus collected was diluted with 0.1 M NaCl in a ratio of 1 g of mucus and 5 mL of NaCl, gently stirred for 1 h on ice, and centrifuged at 10,400 g at 10 °C for 2 h. The supernatant was discarded. The residual mucus was resuspended in half of the volume of 0.1 M NaCl as used for the first purification step and gently stirred on ice for 1 h followed by another centrifugation. The supernatant was discarded and the purified mucus was homogenized before further use [16].

Table 1
Schematic illustration of NLC and SLN excipient composition.

Formulation	Composition			
NLC				
N1	Crodamol GTCC 30 mg	Lipoid S100 18 mg	Paraffin wax 90 mg	PSE_{10} 12 mg
N2	Miglyol 840 43 mg	Lipoid S100 43 mg	Precirol ATO5 43 mg	PSE_{10} 21 mg
SLN				
S1	Capmul GDB 107.2 mg	Pluronic F-127 21.4 mg		PSE_{10} 21.4 mg
S2	Witepsol E85 107.2 mg	Pluronic F-127 21.4 mg		PSE_{10} 21.4 mg
S3	Cetyl Palmitate 83.3 mg	TEGO Care CG90 50 mg		PSE_{10} 16.7 mg
S4	Capmul GDB 41.7 mg	Witepsol E85 41.7 mg	Pluronic F-127 33.3 mg	PSE_{10} 33.3 mg
S5	Capmul GDB 75.0 mg	Pluronic F-127 37.5 mg	T.C. CG90 22.5 mg	PSE_{10} 15.0 mg
S6	Capmul GDB 75.0 mg	Pluronic F-127 22.5 mg	Pluronic F-68 22.5 mg	PSE_{10} 15.0 mg

2.8. Rheological measurements

Rheological measurements were conducted to further investigate the interaction of mucus and NLCs/SLNs formulations. Therefore, 500 μL of purified mucus and 500 μL of prepared NLCs/SLNs dispersion were gently mixed using a spatula. After 4 h of incubation at 37 °C, samples were transferred to a Haake Mars plate-plate rheometer (Thermo Scientific, Vienna, Austria) [16]. All the experiments were made in triplicate.

2.9. Mucus diffusion evaluation

The diffusion properties of nanoparticles into purified porcine intestinal mucus were evaluated using a rotating tube method [18]. Silicon tubes with an inner diameter of 30 mm, each 4 cm in length, were filled with 150 μL of purified porcine intestinal mucus using a 1 mL syringe. Subsequently, 50 μL of the sample, prepared as a 3% (w/v) dispersion of nanoparticles in water, was added at one end, and the tube was sealed with a silicon plug. The tubes were then rotated in an incubator at 37 °C for 24 h under light protection. Afterward, the tubes were frozen at −80 °C and cut into 10 slices of 4 mm, starting from the point where the samples were added. The cut tubes underwent extraction with DMF (500 μL). Next, the samples were centrifuged for 5 min at 9000 rpm using an Eppendorf MiniSpin Centrifuge. The fluorescence analysis of 100 μL of the supernatant was measured in a microplate reader spectrophotometer at 570 nm/610 nm. The results were analyzed as a percentage of the total fluorescence measured in each segment of the cut tube. All the experiments were made in triplicate.

2.10. Cytocompatibility assay

The test was conducted on the Caco-2 cell line. Cytotoxicity of thiolated polymers was investigated on a Caco-2 cell line using a resazurin assay [19]. The samples were prepared at a final concentration of 0.50% (w/v), 0.10% (w/v), and 0.05% (w/v) concentration in HBS pH 7.4. Thereafter, 100 μL each solution was added to the cell culture and then incubated for 3 h at 37 °C. The test solutions were removed and then 150 μL of 0.1 % (w/v) resazurin in HBS solution was added to each well, followed by 3 h of incubation at 37 °C in a 5% CO_2 environment. Finally, 100 μL from each well was transferred to a 96-well plate in the microplate reader spectrophotometer for fluorescence measurements at excitation and emission wavelengths of 540 and 590 nm, respectively. The percentage of cell viability was calculated with the following *Equation (1)*:

$$Cell\ viability\ (\%) = \frac{intensity\ sample - intensity\ of\ negative\ control}{intensity\ of\ positive\ control - intensity\ of\ negative\ control} \quad \text{Equation 1}$$

as a positive control, HBS was used, while a 0.1% v/v Triton-x solution was used as a negative control. All the experiments were made in triplicate.

2.11. Cellular uptake evaluation

The analysis was performed to assess the internalization of the produced formulation in the cells. Caco-2 cell lines were seeded at a density of 2.5×10^4 cells/well in a 24-well plate in 500 μL minimum essential medium and incubated in a 5% CO_2 environment at 37 °C. The medium was changed every 48 h for 14 days. When the confluence of the cell culture reached a value of about 80%, they were washed twice using 500 μL HBS. The samples were prepared at a final concentration of 0.05% (w/v) of LGR-labelled particles in HBS pH 7.4.

After a three-time wash, 500 μL test solutions and HBS as a control, were added to the cell culture and stored in the incubator for 3 h. After removing the NLCs and SLNs with HBS, cells were detached from wells by incubating 150 μL of trypsin for 5 min at 37 °C on cells.

After centrifugation the supernatant was discarded and cell pellets were resuspended in PBS twice. Subsequently, cells were filtered through a cell strainer with 70 μm pore size and diluted with PBS for flow cytometer analysis. Results were expressed in terms of the number of cells that showed high fluorescence after uptake of LGR-labelled NLCs and SLNs. All data were analyzed with FlowJoTM 170 v10.8 [7]. All the experiments were made in triplicate.

2.12. Confocal microscopy

Cell internalization of nanoparticles was further confirmed by confocal microscopy (Leica TCS SP8) with the appropriate filter sets [7, 20]. Briefly, Caco-2 cells were seeded in a density of 1×10^5 cells/ml (3×10^4 cells/well) in an eight-well chamber (μ-slide, Ibidi) for 4 days until 100% confluency was reached. 250 μL of LGR labelled nanoparticles were added to the wells. After 3 h incubation time, Caco-2 cells were rinsed twice with pre-warmed Opti-Mem. The cell nuclei were stained by using Hoechst 33528 at a concentration of 1 μg/mL for 7 min. All fluorescence images were recorded with the same parameters. Image post-processing was performed by Huygens Professionals software: the yz- and xz-projections were prepared from 5 XY images of an image stack at 0.2 μm z-step length. Spectral unmixing was applied to eliminate fluorescence bleed between detection channels due to overlapping emission spectra. Furthermore, 2D image filtering was regulated by using a Gaussian filter [20,21].

2.13. Endosomal escape study

The study focuses on investigating the interaction between red blood cells and nanocarriers to predict the likelihood of nanocarriers exiting the endosomal pathway. Nanocarriers that establish a stronger interaction with the cell membrane are believed to have the potential to disrupt endosomes, facilitating an escape from the endosomal pathway. The haemolysis assay is employed as a method to assess the interaction and evaluate the potential for endosomal escape in nanocarriers [7] In detail, erythrocyte concentrate was diluted 1:100 with sterile HBS pH 7.4. After that, 250 μL of diluted blood was mixed with 250 μL of NLCs/SLNs suspension prepared in HBS with concentrations of 0.5% (w/v), 0.1% (w/v) and 0.05% (w/v). 0.1% (w/v) Triton-X in HBS and HBS mixed with diluted erythrocytes were used as control samples. HBS mixed with erythrocytes served as the negative control. After incubation in a thermomixer at 300 rpm and 37 °C for 3 h, samples were centrifuged at 500 g for 10 min. The absorption of haemoglobin released from the erythrocytes was measured photometrically at 415 nm. The following *Equation (2)* was used to calculate the extent of haemolysis in percentage:

$$\%\ Hemolysis = \frac{Abs\ (T) - Abs\ (neg)}{Abs\ (pos) - Abs\ (neg)} \quad \text{Equation 2}$$

where Abs (T) is the absorbance of the test sample, Abs (neg) is the absorbance of the negative control, and Abs (pos) is the absorbance of the positive control.

3. Results and discussion

3.1. Synthesis and characterization of thiolated $PSE_{10/100}$

^{1}H NMR spectra relating to the thiolation of PSE_{10} are shown in Fig. 2A and will be used as a reference for PSE_{100} and its derivatives for easier interpretation [13]. For both PSE_{10}-SH and PSE_{10}-Cys, although the signals relative to the Cys are hardly visible due to the long PEG chain and the many signals of protons from it, confirmation of successful thiolation is detectable by the disappearance of the -PN group signal in the aromatic zone (Fig. 2B).

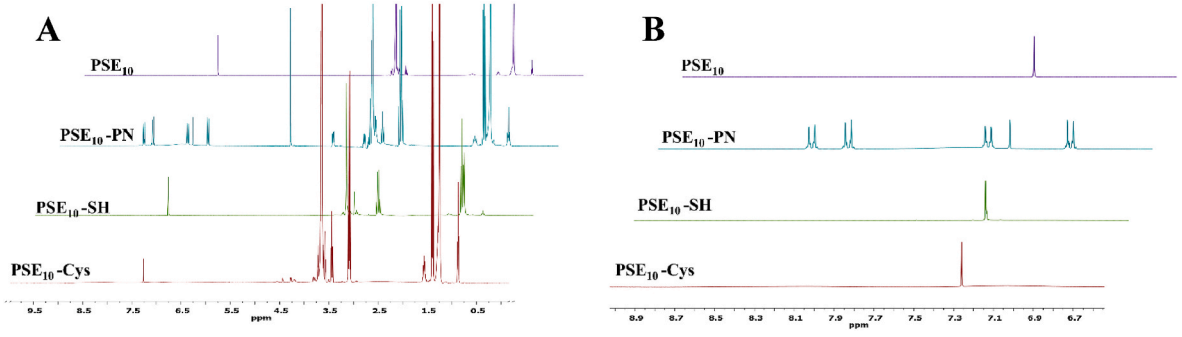

Fig. 2. ^{1}H NMR spectra of PSE_{10} (**A**) and zoom on the aromatic region (**B**).

These results of the coupling with MNA obtained using disulfide and Ellman's test. $PSE_{10/100}$-SH, $PSE_{10/100}$-MNA, and $PSE_{10/100}$-Cys were characterized by quantifying the amount of free and oxidized thiol groups on the polymer backbone. As shown in Table 2, the lower amount of free thiol groups in second- and third-generation products ($PSE_{10/100}$-MNA and $PSE_{10/100}$-Cys), confirmed the success of the synthesis of S-protected $PSE_{10/100}$. In detail, the percentage of disulfide groups detected by the analysis showed the efficacy of the thiol-disulfide reaction used for $PSE_{10/100}$-MNA and, on the other hand, the increased number of S-protected groups once cystine is used in the reaction for $PSE_{10/100}$-Cys. The synthetic process involves free thiol groups protection from disulfide bond formation by MNA and Cys to obtain the second- and third-generation products, respectively, as a result, the -S-S- groups result in higher amounts than the respective –SH groups.

3.2. Preparation and characterization of NLCs and SLNs

NLCs and SLNs were prepared by melt emulsification followed by ultrasonication. The advantage of this method is the simplicity with minimum stressful conditions, the absence of toxic organic solvents, and leads to a very small particle size distribution, which improves the stability and storage properties of NLCs and SLNs [17]. As preliminary study, different formulations were developed using excipients known for their established use in lipid-based formulations and easy commercial availability to evaluate the best-performing oily and wax mixture for incorporating both unmodified PSE10 and the thiolated derivatives.

Combinations of lipids were prepared, and evaluated and the most promising formulations of NLCs and SLNs were used for further studies. The different lipid combinations, for NLCs and SLNs, were evaluated using the PSE_{10}. As shown in Table 3, the formulation N1 proved to be the most promising and was selected for its smaller size. Additionally, six different SLNs combinations were prepared and characterized. Sample S2, among them, emerged as the most favourable choice for further studies due to its size and Polydispersity Index (PDI) values. Notably, S2 was the only formulation that demonstrated constant values for size and PDI over time.

As shown in Tables 4–5, all nanocarriers were prepared at a size below 200 nm, which is advantageous for cellular uptake that decreases for nanocarriers larger than 200 nm [22]. The size of NLCs and SLNs is also a significant factor in their ability to penetrate the mucus gel layer effectively, as particles smaller than 300 nm are transported more efficiently after oral administration [23,24].

SLNs show a smaller size than NLCs and this observation could depend on the different formulations if compared to SLNs with the different lipid phase and surfactant concentration [25]. The PDI was found less than 0.3 in all preparations of NLCs and SLNs, indicating the homogenous distribution of particles [26].

Table 2
Results from Ellman's and disulfide test performed on obtained samples.

SAMPLES	Free thiol groups (μmol/g)	Total thiol group (μmol/g)	Percentage of -S-S- (%)
PSE_{10}-SH	*448.7*	1000.84	55.17
PSE_{100}-SH	81.3	173.15	53.04
PSE_{10}-MNA	1.49	525.98	99.72
PSE_{100}-MNA	2.81	136.86	97.95
PSE_{10}-Cys	1364.1	6173.5	77.91
PSE_{100}-Cys	924	2418.7	61.79

Table 3
Results obtained at DLS in terms of size, polydispersity index, and ζ-potential for all the preliminary tested formulations of NLCs and SLNs.

Formulation	Size ± SD (nm)	PDI ± SD	ζ-potential (mV)
NLCs			
N1	176 ± 3	0.12 ± 0.00	−15.4
N2	200 ± 9	0.15 ± 0,02	−18.00
SLNs			
S1	152 ± 55	0.21 ± 0.06	−0.74
S2	151 ± 5	0.24 ± 0.01	−0.39
S3	156 ± 6	0.23 ± 0.03	−1.06
S4	77 ± 33	0.37 ± 0.03	−0.40
S5	130 ± 7	0.29 ± 0.06	−0.93
S6	159 ± 79	0.26 ± 0.02	−0.92

Table 4
Schematic characterization of N1 NLCs formulated using unmodified or thiolated $PSE_{10/100}$ surfactants.

NLC compositions varying $PSE_{10/100}$ surfactants				Size ± SD (nm)	PDI ± SD	ζ-potential (mV)
Crodamol GTCC	Lipoid S100	Paraffin wax	PSE_{10}	200 ± 9	0.15 ± 0,02	−18.00
			PSE_{100}	196 ± 14	0.13 ± 0,01	−16.10
			PSE_{10}-SH	153 ± 6	0.25 ± 0,02	−53.60
			PSE_{100}-SH	197 ± 7	0.18 ± 0,02	−41.50
			PSE_{10}-MNA	170 ± 3	0.13 ± 0,03	−42.10
			PSE_{100}-MNA	158 ± 10	0.14 ± 0,01	−29.90
			PSE_{10}-Cys	179 ± 8	0.09 ± 0,02	−35.30
			PSE_{100}-Cys	191 ± 11	0.14 ± 0.01	−35.50

Table 5
Schematic characterization of S1 SLNs formulated using unmodified or thiolated $PSE_{10/100}$ surfactants.

SLN compositions varying $PSE_{10/100}$ surfactants			Size ± SD (nm)	PDI ± SD	ζ-potential (mV)
Witepsol E85	PLR F127	PSE_{10}	151 ± 5	0.24 ± 0.01	−0.39
		PSE_{100}	173 ± 12	0.17 ± 0.03	−0.67
		PSE_{10}-SH	157 ± 3	0.23 ± 0.02	−0.40
		PSE_{100}-SH	164 ± 2	0.23 ± 0.01	−0.35
		PSE_{10}-MNA	146 ± 4	0.21 ± 0.01	−0.82
		PSE_{100}-MNA	185 ± 4	0.23 ± 0.01	−0.90
		PSE_{10}-Cys	170 ± 2	0.17 ± 0.01	−36.50
		PSE_{100}-Cys	184 ± 15	0.17 ± 0.02	−34.40

The ζ-potential is a key parameter that determines the net surface charge of colloidal dispersions, and it plays a crucial role in maintaining their physical stability due to the electrostatic repulsion of similarly charged nanoformulations [8]. ζ-potentials of NLCs shift towards more negative values from the unthiolated samples to the thiolated ones, and they increase slightly, moving towards less negative values, in the case of second- and third generation NLCs compared to thiolated products. This observation might be explained by the protection of the thiol group. The difference in surface charge between the lipid-based nanocarriers could be explained by the different excipient adopted for their formulation. In fact, SLNs were prepared using Pluronic F-127, a zwitterionic polymeric surfactant hypothetically able to modulate the charge brought by the PSE surfactant.

NLCs and SLNs labelled with LGR were also characterized by size and PDI in the same way as the unlabelled ones and they showed suitable size and PDI that enable mucus interaction (Tables S1–S2): all nanocarriers were prepared at a size below 300 nm and PDI less than 0.3.

3.3. Rheological measurements

Rheological measurements were adopted to detect changes in the properties of mucin solutions after the dispersion of the above-prepared samples. The interactions between the nanoparticles and intestinal mucosa were examined concerning their dynamic viscosity, as illustrated in Fig. 3. The increased viscosity detectable from unprotected

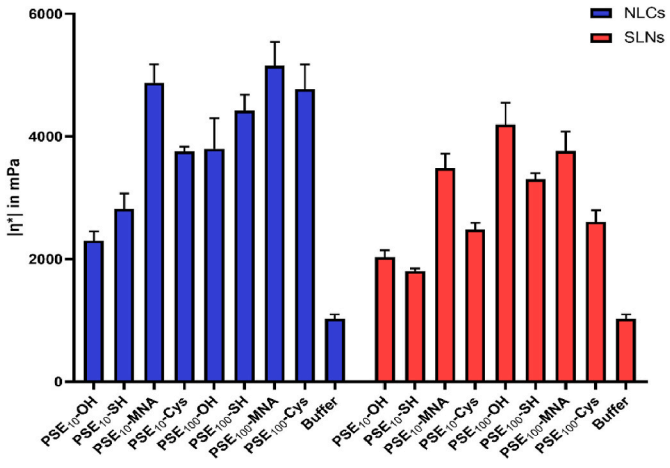

Fig. 3. Mean dynamic viscosity values for the different generations of thiolated $PSE_{10/100}$.

$PSE_{10/100}$-SH-based NLCs/SLNs to $PSE_{10/100}$-based NLCs/SLNs can be attributed to the introduction of thiol-groups. The $PSE_{10/100}$-MNA induced an increase in viscosity compared to the unmodified surfactant and the unprotected thiolated surfactant, respectively. This improvement is due to the interaction between the modified surfactants and mucus, which is mediated by both covalent and non-covalent interactions between the sample and the cysteine-rich domains of mucus [27]. The formation of new disulfide bonds between the surfactant and thiols of mucus occurs immediately after mixing. These results can be explained by the -MNA as a leaving group that preactivated the surfactant for the thiol-disulfide exchange reaction. The presence of a pyridyl substructure with a nitrogen atom results in electron withdrawal, which increases the reactivity of the disulfide bond. As a result, thiols of cysteine-bearing mucus can easily displace MNA [28]. In contrast, NLCs/SLNs formulated by the less reactive $PSE_{10/100}$-Cys indicated a lower viscosity than the NLCs/SLNs decorated with -MNA ligand. Hence, the reduced reactivity of the protection via Cys can be easily observed.

3.4. Mucus diffusion evaluation

The diffusion properties of NLCs and SLNs samples ($PSE_{10/100}$-OH, $PSE_{10/100}$-SH, $PSE_{10/100}$-MNA, $PSE_{10/100}$-Cys) were evaluated by rotating tube method using tubes filled with porcine small intestinal mucus [7,16]. This assay was used to assess the influence of different chemical structures, sizes, and degrees of thiolation on the ability of nanoformulations to cross the mucosal layer. As shown in Fig. 4, the $PSE_{10/100}$-OH NLCs resulted in greater diffusion than thiolated NLCs, leading to less nanoformulation remaining in the first mucosal segments. This behaviour can be explained by the presence in this case of only non-covalent interactions with the mucus membrane, allowing unimpeded diffusion through the mucus layers [29]. The $PSE_{10/100}$-SH NLCs showed less diffusion in the mucus than the other analyzed samples. This result may be due to the reduced penetration of unprotected thiolate polymers into the mucus, attributable to the formation of inter- and intramolecular disulfide bonds. These disulfide bonds could increase the adhesiveness of the thiolated polymers, but may also limit their movement within the mucus layer due to the increased rigidity and size of the created structures [30]. As shown in Fig. 4A, mucus diffusion of the $PSE_{10/100}$-SH NLCs is lower than other thiolated NLCs starting from the third mucous segment.

The greater diffusion of $PSE_{10/100}$-MNA NLCs compared to unprotected samples could be due to the S-protection that protects the surfactant from inter- and intramolecular cross-linking, allowing the formulation to diffuse into the mucus. The greater reactivity of the MNA ligand results in faster covalent interactions with the cysteine portions of the mucus, compared to the less reactive Cys ligand, ultimately leading to less penetration. $PSE_{10/100}$-Cys NLCs showed the greatest diffusivity, reaching the posterior segments to a greater extent than the other generations. Due to their relatively lower reactivity, they allow diffusion into the mucus layer before forming disulfide bonds. By using S-protection with L-cysteine, the thiolated polymers can penetrate the mucus layer more deeply, allowing them to overcome the outer layer of mucus that is constantly being replaced [31].

As shown in Fig. 4B, the mucus diffusion of SLNs was higher than that of NLCs. This behaviour could be related to their relatively smaller size and by the almost neutral ζ-potential if compared to NLCs. In fact, it has been already reported that the use of zwitterionic polymers such as Pluronic F-127 can improve the mucus permeating properties due to the neutral charge and the hydrophilic surface of the DDS [3,32,33]. From the results obtained, it was possible to observe that all samples showed good diffusion within the mucus layers, probably more due to the structure and size of the SLNs than to the different formulations. Again, $PSE_{10/100}$-Cys SLNs showed the best mucodiffusion results, reaching the innermost mucosal layers to greater extent, probably due to the lower reactivity of these formulations with the mucus layer.

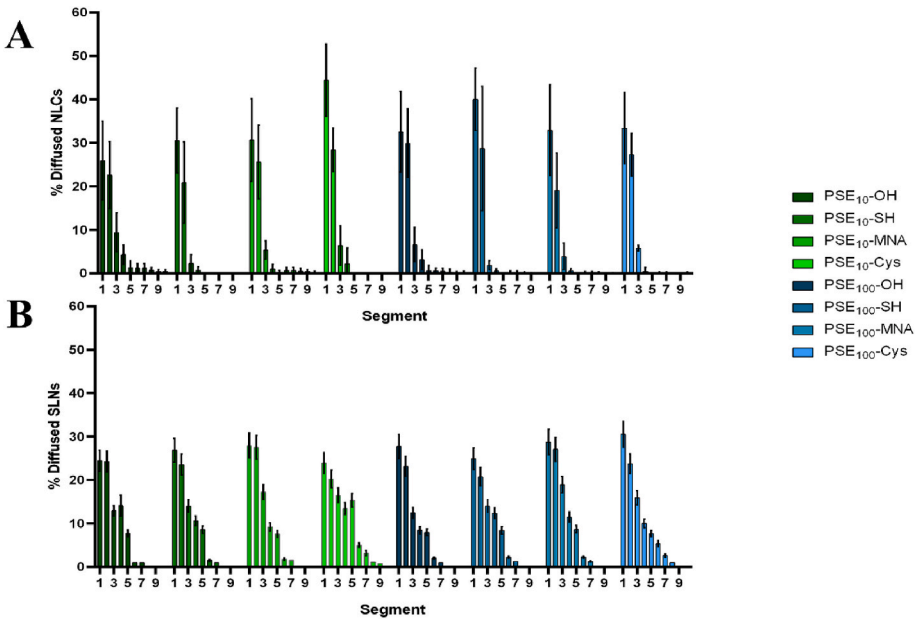

Fig. 4. Diffusion of fluorescence-labelled NLCs (**A**) and SLNs (**B**) through porcine intestinal mucosa, using the rotating tube method.

3.5. Cytocompatibility assay

NLCs and SLNs were evaluated for cytotoxic effects on Caco-2 cells at concentrations of 0.50% (w/v), 0.10% (w/v), and 0.05% (w/v) by resazurin assay.

The results in Fig. 5 showed a viability of over 80% at a concentration of 0.05% (w/v) for both NLCs and SLNs. Therefore, this concentration was considered safe, and further cell studies were conducted at this concentration. Nevertheless, the comparison between NLCs and SLNs showed a higher toxicity of the former than the latter. Viability was above 80% even at a concentration of 0.1% (w/v) for all SLNs but not for NLCs where this result is confirmed only for NLCs decorated with $PSE_{10/100}$-MNA and PSE_{100}-Cys. One explanation for this result could attributed to the higher concentration of surfactant adopted in NLCs when compared to SLNs [34].

3.6. Cellular uptake evaluation

Cellular uptake was evaluated using a flow cytometer and confocal laser scanning microscopy. Results are shown in Fig. 6. The results of PSE_{10}-based NLCs showed the difference in adhesion between the first-, second-, and third-generation products with the adhesion increasing from the first to the third generation, which showed a higher uptake. The better uptake of $PSE_{10/100}$-MNA-based NLCs, compared to the unprotected surfactant $PSE_{10/100}$-SH, could be caused by the S-protection, as already shown for the mucus diffusion of NLC studies performed in this project. One explanation for the increased reactivity of the -MNA ligand could be the quicker covalent interactions with the cysteine portions on the cell surface [28]. In contrast, $PSE_{10/100}$-Cys-based NLCs showed the highest uptake, probably as a result of the relatively high reactivity with cysteine residues present on the cell surface, allowing for a more rapid internalization process of the system within the cell. The cell surface contains multiple exofacial proteins and enzymes, such as

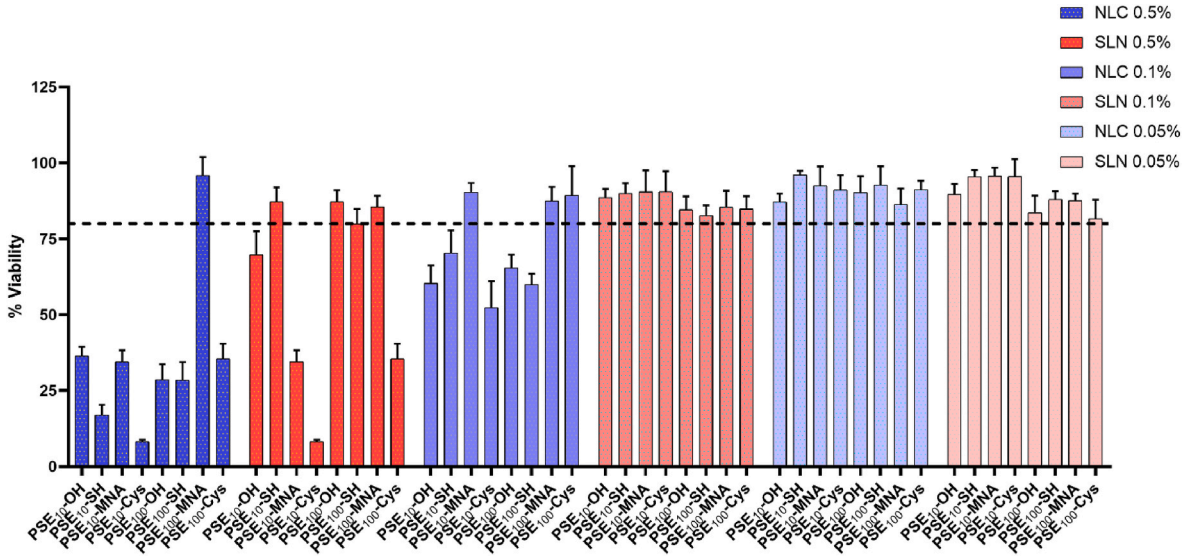

Fig. 5. Viability of Caco-2 cells after treatment with NLCs and SLNs at indicated concentrations. The dotted line at 80% indicates the cytocompatibility limit. Data are means of three experiments ± standard deviation.

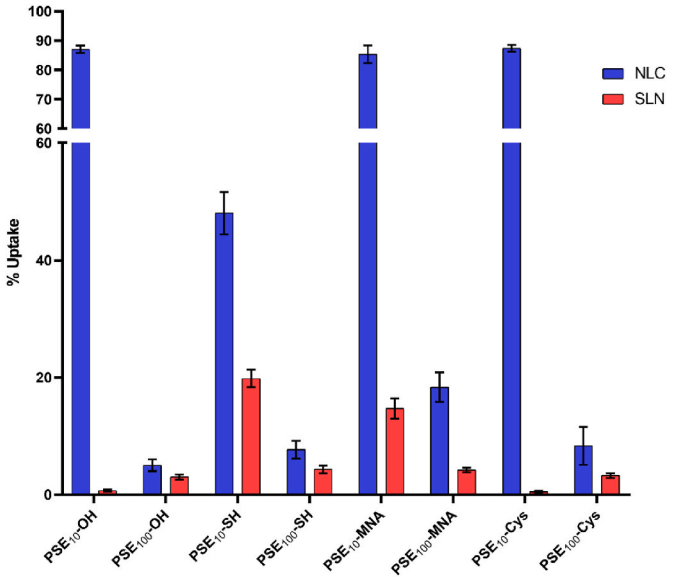

Fig. 6. In vitro cellular uptake of LGR labelled NLCs. Percentage of cells showing a fluorescence signal after cellular uptake of LGR labelled NLCs incubated on cells at a concentration of 0.05% (w/v). Shown data are means of three experiments ± standard deviation.

integrins, scavenger receptors, and protein tyrosine phosphatase, which have cysteine-rich domains that can interact with the thiol groups of obtained samples to form disulfide bonds [18,35]. Furthermore, PSE_{10}-based NLCs showed significantly higher cellular uptake than PSE_{100}-based NLCs, demonstrating the superiority of the shorter PEG chains. This observation is following the already documented shielding effect of the PEG corona formed by a long PEG chain, as described by Ref. [21]. The presence of a PEG corona can decrease cellular uptake of nanocarriers through two mechanisms such as steric hindrance and reduction of electrostatic interactions between the nanocarriers and cells. Therefore, the modification of short PEG chains and the length of the PEG surfactant could be the main factors affecting adhesion. Although SLNs showed lower uptake than NLCs, the thiolation improved the uptake performance. This result confirms that thiolated groups can be involved in the uptake mechanism thanks to the formation of disulfide bonds between the cell's surface and nanoparticles. SLNs formulated with the second-generation products, $PSE_{10/100}$-MNA showed also a higher uptake than the unmodified ones, but the same did not appear in third-generation products. Hence, the desired reduced reactivity induced by the -Cys protection was herein demonstrated. Additionally, the superiority of short PEG chains in SLNs was highlighted, indicating that uptake is largely influenced by the thiolation of short PEG chains and the chain length of the PEG surfactant.

Cellular uptake of nanoparticles was further confirmed taking advantage of confocal laser scanning microscopy which makes sharper images of fluorescently labelled samples.

Thanks to confocal laser scanning microscopy studies, it is possible to show that in the case of PSE_{10}-based NLCs, LGR is only visible around the nuclei (Fig. 7). Therefore, the unmodified NLCs stick only to the cell membrane and were not properly internalized. In the case of PSE_{10}-SH-based NLCs, but especially for PSE_{10}-MNA- and PSE_{10}-Cys-based NLCs, LGR is also detected inside of the nuclei. That means, in the case of thiolated NLCs, internalization, and endosomal escape occurred because NLCs were exited from the endosomes and LGR stays inside the NLC until entering the nuclei of cells.

The results of SLNs obtained by flow cytometer were also confirmed. In particular, SLNs were less internalized than NLCs. Furthermore, it was confirmed that SLNs formulated with first-, second-, and third-generation products, $PSE_{10/100}$-SH, $PSE_{10/100}$-MNA, and $PSE_{10/100}$-Cys, are internalized more than the ones with unmodified surfactant $PSE_{10/100}$. In the case of SLNs formulated with first-, second-, and third-generation products, LGR was inside and outside the nuclei, which means that internalization and endosomal escape occurred.

Live images of Caco-2 cell monolayers having been incubated with 0.05% (w/v) LGR-loaded nanocarrier formulation are displayed in Figs. 7–8. The first column shows the stained nuclei of the cells. The second column in the middle, shows the LGR of the NLCs/SLNs and it is possible to see how well the uptake happened. The third column is an overlay of the other two, the first and second respectively. Moreover, the second and third images related to PSE_{10} NLCs/SLNs are significantly clearer than those of PSE_{100}, confirming the greater internalization and thus the superiority of the short PEG chain.

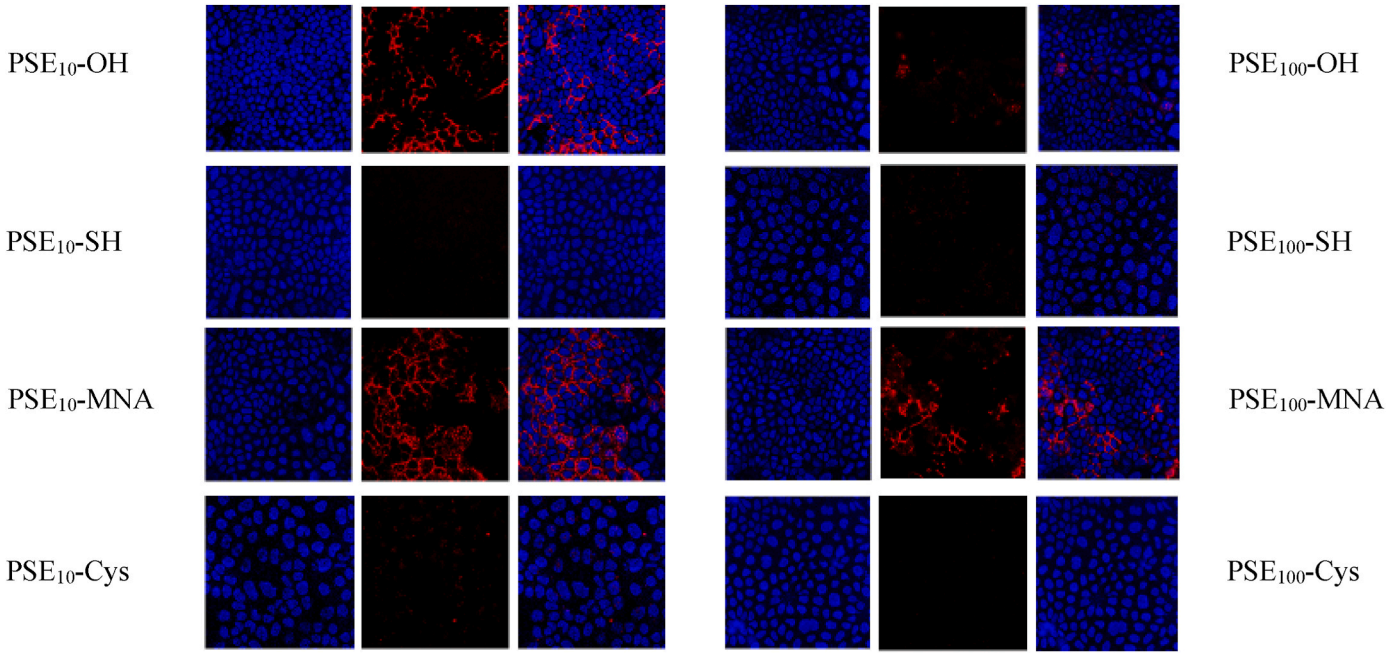

Fig. 7. Cellular uptake of NLCs visualized by confocal microscopy.

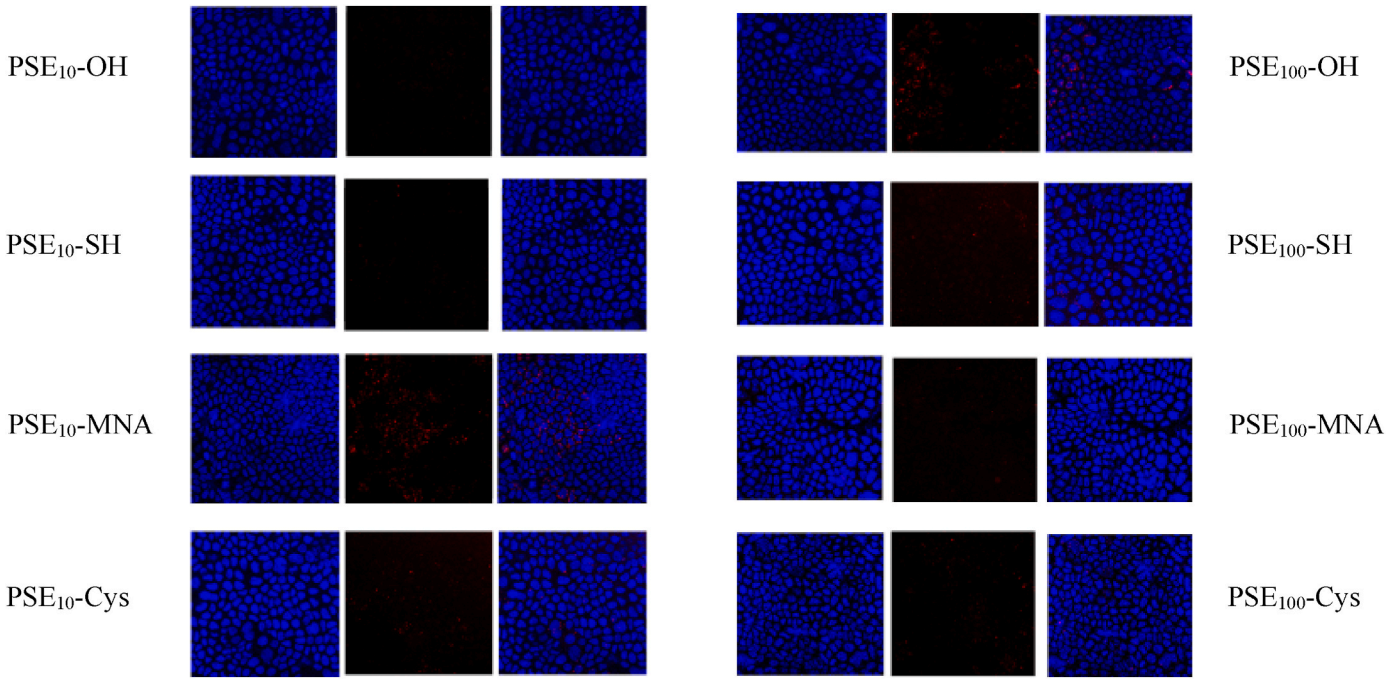

Fig. 8. Cellular uptake of SLNs visualized by confocal microscopy.

3.7. Endosomal escape study

As shown in Fig. 9, there is a clear difference in haemolysis for the first, second, and third generation NLCs decorated with PSE_{10}. The third generation NLCs decorated with PSE_{10}-Cys, showed the highest haemolysis values at all concentrations 0.5% (w/v), 0.1% (w/v), and 0.05% (w/v). Even at the lowest concentration, 72% of the erythrocytes were lysed. That means that they have a high interaction with cell membranes in line with the results of cellular uptake studies. In fact, with the confocal microscope, the presence of LGR was observed around and inside nuclei and that confirmed that endosomal escape occurred.

Furthermore, SLNs have shown a lower capacity for haemolysis. Especially at concentrations 0.1% (w/v) and 0.05% (w/v), there is no haemolysis capacity for all, except for the SLNs with PSE_{10} that have shown 15% of haemolysis. At concentrations of 0.05% (w/v), all SLNs have displayed a haemolysis capacity of 25% or more, which is, however, significantly lower than NLCs. One reason for this result could be the different formulations and concentrations of surfactant between SLNs and NLCs. Therefore, the haemolysis assay showed a higher interaction of NLCs with the cell membrane compared to SLNs, due to the formation of disulfide bonds between the thiols in the cells and those in the nanocarriers. In light of this, the higher cytotoxicity shown by the results obtained from the studies of cytocompatibility performed in this project would find another explanation with NLCs hypothetically being much more cytotoxic likely because of the major interaction with the cell membrane.

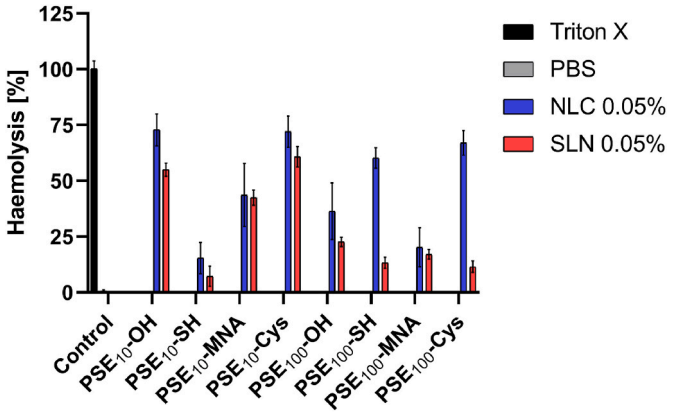

Fig. 9. Haemolysis of erythrocytes concentrate after incubation with NLCs in final concentrations at 0.5% (w/v), 0.1% (w/v) and 0.05% (w/v). Displayed values are means of three experiments ± standard deviation.

4. Conclusion

The accomplishment in surface decoration of NLCs and SLNs allowed to investigate the influence of different S-protected moieties could effectively increase cellular uptake if compared to free thiol groups. Regarding the comparison between NLCs and SLN, the former resulted in being able to permeate the mucus layer. On the other hand, the latter proved to improve cellular uptake and endosomal escape, while demonstrating more difficulties in permeating the mucus. Nevertheless, considering the improved NLC performance in internalization, the relative potential cytotoxicity due to the increased interaction with cell membranes must also be mentioned when compared to the SLNs' one.

As expected, preactivation through MNA protection increased mainly the mucoadhesion properties thanks to the enhanced reactivity for the thiol-disulfide reaction due to the presence of the thionicotinic group. On the other hand, the protection through Cys combined with the lower molecular weight of PSE_{10} allowed obtaining the best performance in terms of synergy among the target properties of this work. In fact, not only demonstrated good mucoadhesive properties, but also the best performances when mucodiffusion is considered. The resulting data on cellular uptake and endosomal escape furtherly confirmed the promising features for the oral drug delivery acquired thanks to Cys S-protection, with an enhanced internalization by intestinal cells and improved stability against degradation by lysosomes due to an enhanced endosomal escape.

CRediT authorship contribution statement

Gennaro Balenzano: Writing – original draft, Data curation, Conceptualization. **Giuseppe Francesco Racaniello:** Writing – original

draft, Methodology, Data curation. **Miriam Domenica Panzarino:** Methodology, Data curation. **Patrick Knoll:** Writing – review & editing, Validation. **Martyna Truszkowska:** Data curation. **Valentino Laquintana:** Formal analysis, Data curation. **Andreas Bernkop-Schnürch:** Writing – review & editing, Validation, Supervision, Conceptualization. **Nunzio Denora:** Writing – review & editing, Validation, Supervision, Project administration, Funding acquisition, Conceptualization.

Declaration of competing interest

The authors declare that they have no known competing financial interests or personal relationships that could have appeared to influence the work reported in this paper.

Data availability

Data will be made available on request.

Acknowledgements

This project was partially funded by Italian University and Research Ministery (PRIN code: 2022PKWPAJ). Gennaro Balenzano is supported by Italfarmacy srl (Trani, Italy). Authors thank Mr. Nicola Di Masi (University of Bari, Bari, Italy) for his skillful technical assistance in recording NMR spectra. Authors also acknowledge Siciliani S.p.A. (Palo del Colle, Italy) for providing the samples for mucoadhesion and diffusion studies. The University of Bari "Aldo Moro" (Bari, Italy) is also gratefully acknowledged for its financial support.

Appendix A. Supplementary data

Supplementary data to this article can be found online at https://doi.org/10.1016/j.jddst.2024.105540.

References

[1] F. Sommonte, I. Arduino, R.M. Iacobazzi, M. Tiboni, F. Catalano, R. Marotta, M. Di Francesco, L. Casettari, P. Decuzzi, A.A. Lopedota, N. Denora, Microfluidic assembly of "Turtle-Like" shaped solid lipid nanoparticles for lysozyme delivery, Int. J. Pharm. 631 (2023) 122479, https://doi.org/10.1016/j.ijpharm.2022.122479.

[2] R.M. Iacobazzi, F. Vischio, I. Arduino, F. Canepa, V. Laquintana, M. Notarnicola, M. P. Scavo, G. Bianco, E. Fanizza, A.A. Lopedota, A. Cutrignelli, A. Lopalco, A. Azzariti, M.L. Curri, M. Franco, G. Giannelli, B.C. Lee, N. Depalo, N. Denora, Magnetic implants in vivo guiding sorafenib liver delivery by superparamagnetic solid lipid nanoparticles, J. Colloid Interface Sci. 608 (2022) 239–254, https://doi.org/10.1016/j.jcis.2021.09.174.

[3] H. Spleis, M. Sandmeier, V. Claus, A. Bernkop-Schnürch, Surface design of nanocarriers: key to more efficient oral drug delivery systems, Adv. Colloid Interface Sci. 313 (2023) 102848, https://doi.org/10.1016/j.cis.2023.102848.

[4] F. Sommonte, I. Arduino, G.F. Racaniello, A. Lopalco, A.A. Lopedota, N. Denora, The complexity of the blood-brain barrier and the concept of age-related brain targeting: challenges and potential of novel solid lipid-based formulations, J. Pharmaceut. Sci. 111 (2022) 577–592, https://doi.org/10.1016/j.xphs.2021.08.029.

[5] W. Shan, X. Zhu, W. Tao, Y. Cui, M. Liu, L. Wu, L. Li, Y. Zheng, Y. Huang, Enhanced oral delivery of protein drugs using zwitterion-functionalized nanoparticles to overcome both the diffusion and absorption barriers, ACS Appl. Mater. Interfaces 8 (2016) 25444–25453, https://doi.org/10.1021/acsami.6b08183.

[6] A. Makhlof, M. Werle, Y. Tozuka, H. Takeuchi, A mucoadhesive nanoparticulate system for the simultaneous delivery of macromolecules and permeation enhancers to the intestinal mucosa, J. Contr. Release 149 (2011) 81–88, https://doi.org/10.1016/j.jconrel.2010.02.001.

[7] P. Knoll, N. Hörmann, N.-M. Nguyen Le, R. Wibel, R. Gust, A. Bernkop-Schnürch, Charge converting nanostructured lipid carriers containing a cell-penetrating peptide for enhanced cellular uptake, J. Colloid Interface Sci. 628 (2022) 463–475, https://doi.org/10.1016/j.jcis.2022.07.160.

[8] G.F. Racaniello, P. Knoll, A.M. Jörgensen, I. Arduino, V. Laquintana, A. A. Lopedota, A. Bernkop-Schnürch, N. Denora, Thiolation of non-ionic surfactants for the development of lipid-based mucoadhesive drug delivery systems, Eur. J. Pharm. Biopharm. 179 (2022) 95–104, https://doi.org/10.1016/j.ejpb.2022.08.015.

[9] P. Knoll, G. Francesco Racaniello, V. Laquintana, F. Veider, A. Saleh, A. Seybold, N. Denora, A. Bernkop-Schnürch, Lipid-based nanoparticles: enhanced cellular uptake via surface thiolation, Int. J. Pharm. 635 (2023) 122753, https://doi.org/10.1016/j.ijpharm.2023.122753.

[10] M. Perrone, A. Lopalco, A. Lopedota, A. Cutrignelli, V. Laquintana, M. Franco, A. Bernkop-Schnürch, N. Denora, S-preactivated thiolated glycol chitosan useful to combine mucoadhesion and drug delivery, Eur. J. Pharm. Biopharm. 132 (2018) 103–111, https://doi.org/10.1016/j.ejpb.2018.09.015.

[11] C.E. Kast, A. Bernkop-Schnürch, Thiolated polymers — thiomers: development and in vitro evaluation of chitosan–thioglycolic acid conjugates, Biomaterials 22 (2001) 2345–2352, https://doi.org/10.1016/S0142-9612(00)00421-X.

[12] K. Netsomboon, A. Jalil, F. Laffleur, A. Hupfauf, R. Gust, A. Bernkop-Schnürch, Thiolated chitosans: are Cys-Cys ligands key to the next generation? Carbohydr. Polym. 242 (2020) 116395 https://doi.org/10.1016/j.carbpol.2020.116395.

[13] J. Shen, Y. Wang, Q. Ping, Y. Xiao, X. Huang, Mucoadhesive effect of thiolated PEG stearate and its modified NLC for ocular drug delivery, J. Contr. Release 137 (2009) 217–223, https://doi.org/10.1016/j.jconrel.2009.04.021.

[14] S. Bonengel, A. Bernkop-Schnürch, Thiomers - from bench to market, J. Contr. Release 195 (2014) 120–129, https://doi.org/10.1016/j.jconrel.2014.06.047.

[15] G.F. Racaniello, V. Laquintana, S. Summonte, A. Lopedota, A. Cutrignelli, A. Lopalco, M. Franco, A. Bernkop-Schnürch, N. Denora, Spray-dried mucoadhesive microparticles based on S-protected thiolated hydroxypropyl-β-cyclodextrin for budesonide nasal delivery, Int. J. Pharm. 603 (2021) 120728, https://doi.org/10.1016/j.ijpharm.2021.120728.

[16] R. Wibel, D.E. Braun, L. Hämmerle, A.M. Jörgensen, P. Knoll, W. Salvenmoser, C. Steinbring, A. Bernkop-Schnürch, In vitro investigation of thiolated chitosan derivatives as mucoadhesive coating materials for solid lipid nanoparticles, Biomacromolecules 22 (2021) 3980–3991, https://doi.org/10.1021/acs.biomac.1c00776.

[17] F. Veider, Z.B. Akkuş-Dağdeviren, P. Knoll, A. Bernkop-Schnürch, Design of nanostructured lipid carriers and solid lipid nanoparticles for enhanced cellular uptake, Int. J. Pharm. 624 (2022) 122014, https://doi.org/10.1016/j.ijpharm.2022.122014.

[18] C. Leichner, M. Jelkmann, A. Bernkop-Schnürch, Thiolated polymers: bioinspired polymers utilizing one of the most important bridging structures in nature, Adv. Drug Deliv. Rev. 151–152 (2019) 191–221, https://doi.org/10.1016/j.addr.2019.04.007.

[19] J. O'brien, I. Wilson, T. Orton, F.Ë. Ois Pognan, Investigation of the Alamar Blue (Resazurin) Fluorescent Dye for the Assessment of Mammalian Cell Cytotoxicity, 2000.

[20] N.M.N. Le, C. Steinbring, B. Le-Vinh, A. Jalil, B. Matuszczak, A. Bernkop-Schnürch, Polyphosphate coatings: a promising strategy to overcome the polycation dilemma, J. Colloid Interface Sci. 587 (2021) 279–289, https://doi.org/10.1016/j.jcis.2020.12.019.

[21] J.D. Friedl, C. Steinbring, S. Zaichik, N.M.N. Le, A. Bernkop-Schnürch, Cellular uptake of self-emulsifying drug-delivery systems: polyethylene glycol versus polyglycerol surface, Nanomedicine 15 (2020) 1829–1841, https://doi.org/10.2217/nnm-2020-0127.

[22] S.A. Kulkarni, S.S. Feng, Effects of particle size and surface modification on cellular uptake and biodistribution of polymeric nanoparticles for drug delivery, Pharm. Res. (N. Y.) 30 (2013) 2512–2522, https://doi.org/10.1007/s11095-012-0958-3.

[23] M. Abdulkarim, N. Agulló, B. Cattoz, P. Griffiths, A. Bernkop-Schnürch, S. Gómez Borros, M. Gumbleton, Nanoparticle diffusion within intestinal mucus: three-dimensional response analysis dissecting the impact of particle surface charge, size and heterogeneity across polyelectrolyte, pegylated and viral particles, Eur. J. Pharm. Biopharm. 97 (2015) 230–238, https://doi.org/10.1016/j.ejpb.2015.01.023.

[24] S.K. Lai, Y.Y. Wang, J. Hanes, Mucus-penetrating nanoparticles for drug and gene delivery to mucosal tissues, Adv. Drug Deliv. Rev. 61 (2009) 158–171, https://doi.org/10.1016/j.addr.2008.11.002.

[25] S. Alarifi, D. Ahmad, M.E. Omer, M.A. Albekery, K.T. Alharbi, S. Alarifi, D. Ahmad, M.E. Omer, S. Massadeh, A.E. Yassin, Optimization of a Nanostructured Lipid Carriers System for Enhancing the Biopharmaceutical Properties of Valsartan, 2017. https://www.researchgate.net/publication/317065465.

[26] M. Danaei, M. Dehghankhold, S. Ataei, F. Hasanzadeh Davarani, R. Javanmard, A. Dokhani, S. Khorasani, M.R. Mozafari, Impact of particle size and polydispersity index on the clinical applications of lipidic nanocarrier systems, Pharmaceutics 10 (2018), https://doi.org/10.3390/pharmaceutics10020057.

[27] P. Prasher, M. Sharma, S.K. Singh, M. Gulati, N.K. Jha, P.K. Gupta, G. Gupta, D. K. Chellappan, F. Zacconi, T. de Jesus Andreoli Pinto, Y. Chan, G. Liu, K.R. Paudel, P.M. Hansbro, B.G. George Oliver, K. Dua, Targeting mucus barrier in respiratory diseases by chemically modified advanced delivery systems, Chem. Biol. Interact. 365 (2022) 110048, https://doi.org/10.1016/j.cbi.2022.110048.

[28] P. Knoll, N.-M.N. Le, R. Wibel, R.A. Baus, G. Kali, M.H. Asim, A. Bernkop-Schnürch, Thiolated pectins: in vitro and ex vivo evaluation of three generations of thiomers, Acta Biomater. 135 (2021) 139–149, https://doi.org/10.1016/j.actbio.2021.08.016.

[29] V.M. Leitner, G.F. Walker, A. Bernkop-Schnürch, Thiolated polymers: evidence for the formation of disulphide bonds with mucus glycoproteins, Eur. J. Pharm. Biopharm. 56 (2003) 207–214, https://doi.org/10.1016/S0939-6411(03)00061-4.

[30] H.T. Lam, G. Leonaviciute, O. Zupančič, A. Bernkop-Schnürch, Thiomers: impact of in situ cross-linkers on mucoadhesive properties, Eur. J. Pharmaceut. Sci. 106 (2017) 41–48, https://doi.org/10.1016/j.ejps.2017.05.051.

[31] I. Shahzadi, A. Fürst, Z.B. Akkus-Dagdeviren, S. Arshad, M. Kurpiers, B. Matuszczak, A. Bernkop-Schnürch, Less reactive thiol ligands: key towards highly mucoadhesive drug delivery systems, Polymers 12 (2020), https://doi.org/10.3390/POLYM12061259.

[32] D. Chen, D. Xia, X. Li, Q. Zhu, H. Yu, C. Zhu, Y. Gan, Comparative study of Pluronic® F127-modified liposomes and chitosan-modified liposomes for mucus penetration and oral absorption of cyclosporine A in rats, Int. J. Pharm. 449 (2013) 1–9, https://doi.org/10.1016/j.ijpharm.2013.04.002.

[33] F. Veider, P. Knoll, A.M. Jörgensen, D. Stengel, A. Bernkop-Schnürch, Oral drug delivery: influence of mucus on cellular interactions and uptake of lipid-based nanocarriers in Caco-2 cells, Acta Biomater. 167 (2023) 416–424, https://doi.org/10.1016/j.actbio.2023.06.005.

[34] Z. Ujhelyi, F. Fenyvesi, J. Váradi, P. Fehér, T. Kiss, S. Veszelka, M. Deli, M. Vecsernyés, I. Bácskay, Evaluation of cytotoxicity of surfactants used in self-micro emulsifying drug delivery systems and their effects on paracellular transport in Caco-2 cell monolayer, Eur. J. Pharmaceut. Sci. 47 (2012) 564–573, https://doi.org/10.1016/j.ejps.2012.07.005.

[35] Q. Laurent, R. Martinent, B. Lim, A.-T. Pham, T. Kato, J. López-Andarias, N. Sakai, S. Matile, Thiol-mediated uptake, JACS Au 1 (2021) 710–728, https://doi.org/10.1021/jacsau.1c00128.